***iMAX* FRET (I**nformation **Max**imized **FRET**) for multipoint single-molecule structural analysis

Bhagyashree S. Joshi[a], Carlos de Lannoy[a], Mark Howarth[b,c], Sung Hyun Kim[a,d*], Chirlmin Joo[a,d*]

[a]Kavli Institute of Nanoscience, Department of Bionanoscience, Delft University of Technology, Delft, The Netherlands

[b]Department of Biochemistry, University of Oxford, South Parks Road, Oxford OX1 3QU, UK

[c]Current address: Department of Pharmacology, University of Cambridge, Tennis Court Road, Cambridge, CB2 1PD, UK

[d]Department of Physics, Ewha Womans University, Seoul 03760, Republic of Korea

* Corresponding authors:
Sung Hyun Kim, S.H.Kim@tudelft.nl;
Chirlmin Joo, c.joo@tudelft.nl

Abstract

Understanding the structure of biomolecules is vital for deciphering their characteristics and roles in biological systems. While current structural analysis techniques like nuclear magnetic resonance and X-ray crystallography excel in many aspects, they fall short in capturing comprehensive single-molecule information. To address this limitation and to better capture the heterogeneity and dynamic range of biomolecular reactions, there is a need for single-molecule structural analysis tools. To achieve this, we introduce iMAX FRET, a one-pot FRET-based single-molecule method integrated with geometrical 3D reconstruction, offering comprehensive *ab initio* structural analysis. Through the stochastic exchange of fluorescent weak binders, iMAX FRET allows simultaneous assessment of multiple spatial coordinates on a biomolecule within a few minutes of time to generate distinct FRET fingerprints for 3D structural profiling. We demonstrate a mathematical approach for *de novo* structural prediction using iMAX data, opening avenues for native biomolecule analysis. Furthermore, this method facilitates the investigation of conformational changes in individual molecules, illuminating single-molecule structural dynamics. Our technique has the potential to emerge as a powerful approach to advance our understanding of biomolecular structures.

Keywords

Single-molecule FRET, single-molecule structural analysis, single-molecule conformational analysis, computational structure prediction, programmable DNA binding

Introduction

Three-dimensional structure dictates the characteristics and functions of biomolecules[1], and thus their analysis is fundamental to understanding their biological functions. Seemingly small perturbations—a single amino acid substitution, a change in local temperature, or an interaction with other molecules—can lead to a change in structure, which may ultimately lead to diseased cellular states[2-6]. As structure may differ from one protein molecule to another, analyzing the structures of individual single molecules and complexes is a prerequisite to understanding all cellular functions. However, traditional analysis techniques such as nuclear magnetic resonance and X-ray crystallography determine only the ensemble-averaged structure[7,8] and thus are unable to capture the structure variation of individual molecules that may underpin crucial biological processes. Furthermore, they often impose artificial physical conditions during measurements (such as crystallization)[9-11 10] and require complex methodology[12,13]. Single-molecule fluorescence resonance energy transfer (smFRET) and single-particle cryo-electron microscopy have emerged as cutting-edge techniques for interrogating structures of individual molecules. While complex workflow and heavy reliance on specialized experts of single-particle cryoEM hampers its cross-domain adaptability, smFRET is arguably less complex in its execution. smFRET can sensitively measure distances between fluorescent dye pairs attached to a biomolecule of interest in 2-10 nm range at sub-nanometer resolution and has been successfully used for conformational and kinetics analyses of biomolecule structures[14,15]. However, due to the complexity of signals, only one or two dye-labeled points in a single molecule can be tracked at a time[16], precluding a comprehensive understanding of the three-dimensional perspective on the structure without prior knowledge of the molecular structure obtained by other means.

Extensions of conventional smFRET, which allowed observation of multiple distances between a single reference point and several other positions in a molecule of interest using a scheme of DNA exchange, were developed by several groups[17-19]. Although this multi-point analysis mitigated the limitation of the conventional smFRET, the necessity of a single reference point still implied that positions in three-dimensional space could not be triangulated for *de novo* structural reconstruction. We now present information MAXimized FRET (iMAX FRET), a one-pot experimental method to measure all possible mutual distance information between multiple selected points in a single molecule. Unlike hitherto reported FRET-based structural biology methods which require prior structural knowledge, iMAX FRET is the first method that enables *ab initio* structural analysis solely from smFRET data. Using our newly developed software pipeline, we show that iMAX FRET data can be used to determine up to six distances from four positions in 3D space, from which the conformation of a molecule can be reconstructed by geometrical modeling.

Results

The principle of iMAX FRET

iMAX FRET uses weak binders to rapidly assess multiple points in native biomolecules and heteromeric complexes (Fig. 1). In this work, we used short single-stranded DNA (ssDNA) as weak binders to exploit its programmable binding kinetics. Multiple positions of interest in protein, nucleic acid nanostructure, or multimeric complex were labeled with ssDNA molecules (hereafter called docking strand). Docking strands transiently hybridize with imagers – complementary DNA oligos in solution, labeled with either a donor or acceptor fluorophore (Fig. 1a). As these imager binding events occur stochastically and as each docking strand can serve as both the donor and acceptor binding site, all distances between the target positions can eventually be deduced from all the single-pair FRET events in which only a single donor and acceptor imager pair is bound to the target biomolecule. The lengths and concentrations of the imagers were tuned such that only one FRET pair is observed for a significant fraction of recording time. Collected FRET values are subsequently translated to distances, which are then fit together in a three-dimensional construct (Fig. 1b); all possible three-dimensional constructs using these lengths are generated, and the construct that violates the originally measured lengths the least is considered the correct fit. This approach obtains a per-molecule three-dimensional reconstruction without any prior knowledge of the identity or structure of the molecule; only basic geometry rules are applied.

An advantage of iMAX FRET is its relative ease of implementation. A single round of standard two-color FRET measurement is sufficient to obtain all the structural information, whereas other single-molecule methods for multiple distance observation require the inclusion and observation of more dye colors, repeated measurements with probe exchange, or multiple sample preparations with different labeling schemes[16,19-23]. Furthermore, no orthogonal labeling schemes for different positions are necessary, as all positions can be labeled in the same way – with the same type of docking DNA strands, which are all stochastically visited by the same type of probes – here, imager DNA strands.

iMAX FRET can delineate single-stranded DNA profile

As a first step, with a simple example of a ssDNA carrying multiple docking sequences, we sought to check the feasibility of the simultaneous multi-distance measurement with the one-pot stochastic probe exchange scheme. We prepared four ssDNA targets each of which contains two or three interspaced copies of an otherwise identical docking sequence at different positions, designated A, B, and C (Extended Data Fig. 1a, for sequences refer to Supplementary Table 1). Simultaneous binding to positions A and B – spaced 12 nt apart – was expected to give high FRET, positions B and C were spaced 19nt apart which should generate an intermediate FRET, and lastly, the summed 31nt distance between positions A and C should result in a low FRET signal (Extended Data Fig. 1a).

After immobilizing the ssDNA targets on a quartz slide glass via a biotin-streptavidin linkage, a mixture of donor and acceptor imagers of 8nt was added to the sample chamber. The 8nt imager, of which binding dwell time was $\tau_{binding}$=1.0 $\pm$ 0.1 s, was adapted from our previous study[19]. We added 10-fold excess of acceptor-labeled imagers over donor-labeled imagers to increase the probability of both fluorophores being present simultaneously. We then collected all the binding events from the time traces of individual molecules (Extended Fig. 1b) and built a histogram of the averaged FRET value per event (Extended Fig. 1c). All four

DNA samples showed the expected FRET efficiencies of 0.73 ± 0.01, 0.52 ± 0.01, and 0.21 ± 0.02 for positions A, B, and C, respectively (Extended Data Fig. 1c). Notably, the DNA sample carrying all three docking sites showed all three peaks, confirming that our stochastic exchange scheme was capable of simultaneous multi-point assessment.

We noted that most binding events, however, showed FRET efficiency of 0.0 (star, peak area of ~69 %) indicating that donor-only binding events are still dominant in the current experimental condition (Extended Data Fig. 1c). We anticipated that the acquisition of sufficient FRET events, i.e. simultaneous binding of a donor and an acceptor imager, required fine-tuning of the binding kinetics of the two imagers; event duration controlled by imager strand lengths, and event frequency controlled by concentrations of the two imagers. Using Monte Carlo simulations of our experiment (see Supplementary Methods) under different levels of concentration and binding dwell time of imagers, we inferred that 10-fold acceptor excess combined with longer acceptor binding times produced the optimal number of single FRET-pair events (Extended Data Fig. 1d and e). We extended the imager docking strands to 9nt and found that viable FRET events significantly increased compared to the same-length imagers (Fig. 2a-c, Extended Fig. 1f-g). This demonstrated that careful rational design of imager lengths, and hence dwell times, is pivotal in resolving multiple targets in iMAX FRET.

iMAX FRET can resolve DNA nanostructures

To demonstrate iMAX FRET's capability of *ab initio* three-dimensional structure determination, we analyzed a quadrangular DNA nanostructure outfitted with a docking strand at each angle (Fig. 3a, left). The six different distances in this nanostructure, referred to as D1 to D6 (Fig. 3a, right), could be probed with four identical docking strands in iMAX FRET. In this demonstration, however, we prepared each docking strand with a unique sequence for control purposes.

First, we probed each distance by adding two different imager strands simultaneously, which resulted in a single FRET peak per experiment (Fig. 3b). We found that D3 and D5 were well-discernible from the other distances (FRET efficiency mean ± standard deviation of 0.83 ± 0.01 and 0.18 ± 0.01, respectively). D1, D2, D4, and D6 generated highly similar FRET values (0.35 ± 0.01 and 0.30 ± 0.01, 0.45 ± 0.01 and 0.37 ± 0.01, respectively). Then, we increased the complexity by adding 3 imager strands, which allowed simultaneous analysis of three distances. Indeed, for each of the four possible triangles in this quadrangle, we could identify the expected number of FRET peaks (Fig 3c, panels i-iv). Triangle i (constructed from D1, D2, and D6) showed one major peak whereas for ii (D3, D4, and D6) two peaks overlapped, which was expected based on single-distance analysis results. Triangles (iii) and (iv), as expected, showed three peaks for (D1, D4, D6), and (D2, D3, D5), respectively.

To reconstruct the relative coordinates of dyes from per-molecule FRET values, each FRET efficiency E must first be translated to a distance R, following the sixth-power relation between R and E, and this requires estimating the Förster distance (R_0) for our measurement conditions. This parameter combines the influence of dye and medium properties, and relative dye orientations. To estimate R0, we sought to utilize the known structure of double-stranded DNA. First, we prepared DNA nanostructures with one of the docking sites positioned at different locations along one arm of the nanostructure (Extended Fig. 4a-b) and probed two docks simultaneously. As expected, FRET values gradually decreased as we placed

the variable docking site further from the fixed docking site (Extended Fig. 4c-e). We then probed an additional fixed docking site (i.e. three docks per nanostructure) and measured FRET distances for triangles, thus obtaining either two or three expected FRET *E* populations per molecule depending on the degeneracy in the FRET spectrum (Extended Fig. 4f). We could then estimate R_0 by adjusting the value such that all triangles could be aligned by their fixed docks and with their variable dock in the position predicted from the dsDNA geometry (Extended fig. 4g and Supplementary Table 2; see also *DNA structure modeling for Förster radius fitting* in Supplementary Methods) Subsequently, FRET efficiencies were converted to distances using this fitted R_0.

Having acquired the distances, the reconstruction of triangle coordinates is trivial as only one dissimilar triangle (i.e., ignoring rotation, translation, and reflection) can be constructed given the lengths of all three edges. Aligning and averaging triangle coordinates of all single molecules (Extended Fig. 2a), produced the shapes of the four triangle types (Extended Fig. 2b). To demonstrate that triangles reconstructed for single molecules contain sufficient information to allow recognition, we encoded the coordinates in a rotation-, translation- and reflection-invariant embedding[24] and trained a tree-based machine learning algorithm to recognize each type. On held-out molecules, this classifier attained an accuracy of 74%, confirming that spatial reconstruction contains discriminative information (Fig. 3d). Most errors were made between triangles that were expected to show more similarity due to the nanostructure's assumed symmetry (i+iii, ii+iv respectively). Even so, the classifier still correctly assigned classes to most molecules, thus we suspected that the nanostructure is not truly symmetric.

Finally, we probed all six distances simultaneously by adding four different imagers together (Fig. 3c, bottom plot). We observed four peaks. The highest peak at E=0.84 and the lowest at E=0.18 represented D3 and D5 respectively. The other two peaks were, however, not straightforward to assign due to the overlapping FRET values of the other four distances D1, 2, 4, and 6. Nevertheless, the broad peak at 0.38 could be assigned as a degenerate peak of D1, D2, and D6, while the peak at E=0.55 likely arose from D4. FRET values obtained from this experiment were then used to reconstruct a 3D quadrangle. In theory, 30 dissimilar quadrangles can be constructed given the lengths of all six edges. However, not all quadrangles can necessarily be built without violating the given lengths. We therefore wrote an analysis pipeline (see Supplementary Methods) that builds all possible dissimilar quadrangles and chooses the one for which the edge lengths are required to change the least to fit. We found that a 3D quadrangle could be constructed satisfying all distances without violating the FRET-derived lengths (Extended Fig. 3). Similar to the triangle measurements, this reconstruction indicated that the nanostructure has an asymmetric conformation, possibly reflecting the slight out-of-plane attachment positions of the docking strands due to the helical structure of the double-stranded DNA. Also, spatial hindrances due to electrostatic repulsion from the DNA nanostructure might have influenced the actual positions of the docking and imager strands, which could push the dyes further away from the attachment point depending on the local 3D geometry.

In summary, iMAX FRET could successfully demonstrate the structural analysis of up to 4 points in a complex DNA nanostructure, and we could predict and retrieve these structural identities with high accuracy based on FRET fingerprints and computational modeling. This

demonstrates that we could expand the signal space to 6 peaks (considering degenerate peaks) in a one-pot reaction requiring less than 2 minutes without using solution exchanges[19].

iMAX FRET locates the biotin pockets in tetravalent and divalent streptavidin structures

As iMAX FRET is well-suited to determine the relative position of three or more points in space, we set out to study multimeric structures, which are difficult to analyze with traditional FRET due to the inability to control labeling with donor and acceptor fluorophores of subunits within a multimeric protein[25]. Structural analysis of multimeric proteins by other techniques, including mass spectrometry, often requires complex stabilization using chemical linkers or cross-linking[26-29]. In contrast, iMAX FRET can be applied on native complexes. Moreover, ligand-binding multimers present a unique possibility for iMAX FRET. For example, we can use docking strand-conjugated ligands to probe the positions of their binding pockets. We chose streptavidin as our model protein, as it contains four pockets for biotin. This also allowed us to indirectly immobilize streptavidin to a surface, by occupying one of its pockets with an immobilized biotinylated docking strand (Extended Fig. 5a). The other pockets were occupied by docking strands added in solution.

Streptavidin is a tetramer organized in a tetrahedral (D2) symmetry with four biotin-binding pockets (Extended Fig. 5b) First, to derive single distances from four binding pockets, we measured two divalent streptavidin mutants – 1,3 *trans* and 1,2 *cis* which have only two active biotin binding pockets[30] (Fig. 4a and b). As expected, a high FRET peak (0.89 $\pm$ 0.04) was observed for 1,2 *cis* and a mid-FRET peak (0.56 $\pm$ 0.02) for 1,3 *trans* (Fig. 4a and b). Changing the dye positions from one end to another of the imagers proportionately reflected the changes in the FRET values, showing the ability of iMAX FRET to pinpoint the biotin binding pockets accurately (Extended Fig. 5c and d). Subsequent iMAX FRET analysis on the wild-type streptavidin with four active binding pockets showed three different FRET efficiencies of 0.28 $\pm$ 0.02, 0.58 $\pm$ 0.04, and 0.94 $\pm$ 0.04 seen for pockets 1, 2, and 3, respectively (Fig. 4c). Although, in general, six distances were expected from four points, the symmetric tetramer structure of streptavidin could exhibit only three peaks due to degeneracy. Nevertheless, by using these FRET values, we were able to reconstruct the relative positions of the binding pockets (Fig. 4d). The reconstructed 3D spatial coordinates fit the known streptavidin structure gratifyingly well, accounting for a realistic average linker length of 1.8nm, and showed limited variability over 1000 bootstrap iterations (standard deviation of 2.75Å averaged over all four positions, Fig. 4e). This confirms that iMAX FRET is capable of extracting three-dimensional features from multimeric proteins without the aid of complementary methods or additional information on the target.

iMAX FRET has a potential for studying permanent protein conformational changes

Finally, we explore the possibility that the stochastic DNA probe-based detection scheme used in iMAX FRET is also compatible with studying conformational changes of proteins without disturbing their activity. Many proteins undergo profound conformational changes upon binding to a ligand. A well-known example is substrate binding domain (SBD)[31] which captures extracellular substrates and delivers them to transporters. We focused on the SBDs of one such transporter, GlnPQ from *Lactococcus lactis*, which are involved in amino acid sensing and import of asparagine and glutamine[32,33]. Here, we attempted to detect the open-to-closed conformational switch after ligand binding to SBD2 protein[34,35].

We prepared a wild-type protein that can bind glutamine and asparagine and a null mutant that does not bind any ligand as a control[35] (Extended Data Fig. 6a). For DNA labeling, two cysteines were inserted into both proteins at strategic positions each located at one of the two lobes in SBD2 (Extended Data Fig. 6b). These modifications are known to have no adverse effects on their function[35] and the distance between these two positions undergoes a significant change after a ligand binding according to the crystal structures[34]. Indeed, observed FRET increases from 0.25 to 0.40 and from 0.25 to 0.30 upon binding of Glutamine and Asparagine, respectively (Extended Fig. 6c). The smaller FRET shift with Asparagine reflected the fact that SBD2 undergoes a higher conformational change when bound to Glutamine compared to Asparagine[35]. In contrast, we did not observe a FRET shift from the mutant, confirming the FRET shift is indeed induced by ligand binding (Extended Data Fig. 6d). We conclude that iMAX FRET with the stochastic DNA probe exchange method can be applicable to dynamic structural analysis of proteins as a response to stimuli.

Discussion

Here we presented iMAX FRET, a novel structural analysis tool to probe multiple pairwise distances by using high-resolution smFRET and weakly interacting probe scheme. By directly integrating it with geometrical modeling for structural prediction, iMAX FRET enables the assessment and prediction of molecular structures based on their FRET fingerprints with the ultimate sensitivity of a single molecule, thus opening avenues for new *ab initio* structural prediction and conformational dynamics studies.

iMAX FRET has many advantages over established techniques. *a) Short time required for measurement*: As we use the stochastic exchange scheme for probing all possible points in a molecule with otherwise identical probes, this one-pot method cuts down the imaging time considerably as compared to other DNA hybridization-based imaging techniques [19,23,36]. The probe-labeled samples can be practically prepared in 24 hours [19] while weak-binder based fluorescence measurement takes as little as two minutes. Thus, the structural analyses of protein and complex mixtures can be obtained multiple times faster than other structural analysis techniques. *b) Ease of sample preparation*: iMAX FRET overcomes challenging sample preparation or crystallization as required for CryoEM and X-ray crystallography. As only picomolar-range quantities are required for the analyses, it is possible to analyze the most precious samples (e.g. patient materials). The stochastic nature of iMAX FRET measurement makes the sample preparation easier as only one type of attachment chemistry is used for all the docking sites. If necessary, orthogonal labeling and pull-down methods such as His-tag or N-terminus labeling[37] may be used to make the technique more easily accessible and applicable.

iMAX FRET allows probing of multiple distances in a nano object, including complex DNA nanostructures, proteins, and heteromeric complexes of biomolecules. It paves the way for studying the static and dynamic structural analysis on challenging multimeric proteins such as transcription factors and transmembrane proteins. iMAX FRET has the potential to provide quantitative information on the species abundance of multimers and their characteristics in a complex mixture of homo and heteromers. Thus, it can replace cumbersome biochemical assays used to delineate the differential populations of homomers and heteromers present in a particular solution.

Even with its empirical simplicity, iMAX FRET can provide useful 3D structural information of biomolecules. Yet, certain problematic proteins, such as those 1) with too large or complicated structures, 2) with too low or high number of possible labeling points, or 3) with too much degeneracy in the measured distances, may be analyzed over multiple rounds of measurements by utilizing the programmable nature of a probe. Further developments should, therefore, include identifying and evaluating widely appliable methods for the orthogonal labeling of docking strands or the use of other weak binders that do not require protein labeling. A logical first step of labeling to this end is the targeting of cysteine residues[38], which are rare amino acids and are primarily surface-exposed, making them immediately amenable for use in iMAX FRET. Our technique can also be extended to other amino acids such as lysine of which conjugation chemistry is well established[39]. This extension may open the possibility to structures that are difficult to assess using CryoEM and X-ray crystallography or predict with Alpha-fold due to their intrinsic disorder[40] or propensity to irregularly aggregate, or change structure during complex experimental workflows.

Author Contributions

B.S.J. and C.J. initiated and designed the project. B.S.J. and S.H.K. designed and performed the experiments. I.W. expressed and purified the proteins. S.H.K. designed and ran FRET efficiency extraction workflows and Monte Carlo simulations. C.L. designed and ran 3D modeling and structure classification pipelines. M.H. provided the streptavidin mutants. B.S.J, C.L., S.H.K., and C.J. wrote and edited the manuscript. All the authors read and approved the manuscript.

Acknowledgments

We thank Mike Filius for his generous help with the DNA constructs and overall scientific advice. C.J. is supported by The Netherlands Organization for Scientific Research (NWO) (Vici), the European Research Council (an ERC Consolidator grant, 819299), Basic Science Research Program (NRF), and Frontier 10-10 (Ewha Womans University). M.H. acknowledges funding from the Biotechnology and Biological Sciences Research Council (BBSRC, BB/I006303/1).

Declaration of interests

C.J. and B.S.J. have filed a patent for single-molecule protein characterization.

Data availability

The data supporting the findings of this study are available in the article and its supplementary information. Any additional data is available from the main corresponding author upon reasonable request.

Code availability

The iMAX FRET analysis pipeline and additional custom analysis codes are documented and freely available at https://github.com/cvdelannoy/iMAX-FRET.

Materials and Methods

Protein expression and purification

Divalent streptavidins were expressed in *Escherichia coli*, refolded from inclusion bodies, and purified by ammonium sulfate precipitation and ion-exchange chromatography, as reported in the original paper[30]. Tetravalent recombinant (wild-type) streptavidin was procured from Thermo Scientific. Plasmids encoding SBD2 (T369C/S451C) and SBD2 (T369C/S451C/D417C)[34]

were a generous gift from Prof. Bert Poolman (Department of Biochemistry, University of Groningen, The Netherlands), and the proteins were expressed and purified using the reported protocol [34].

Protein labeling

Cysteine labeling was carried out as reported previously[34] with slight modifications as follows. Cysteine residues of purified proteins (25uM in the total volume of 50ul In PBS) were reduced with 50mM Tris(-2-carboethyl)phosphine (TCEP) at 40-fold molar excess for 30 minutes. Excess TCEP was removed with ZebaTM Spin desalting columns 7kDa MWCO (ThermoFisher) as it may interfere with the Maleimide reaction[41]. The proteins were then labeled with 25-fold molar excess monoreactive maleimide-Dibenzocyclooctyne (DBCO) (Sigma Aldrich) in Phosphate Buffered Saline (PBS) pH 7.4 overnight at room temperature. Excess maleimide-DBCO was removed with Zeba columns and reacted with 10-fold molar excess (ratio 1:10, cysteine to linker) of monoreactive Azidobenzoate-(5') functionalized DNA in PBS pH 7.4 and incubated overnight at room temperature.

Single-molecule Setup

All iMAX-FRET measurements were performed on a custom-modified prism-type TIRF microscopy setup built around an inverted fluorescence microscope (Nikon, Ti2e)[42]. For illumination of samples immobilized on a quartz slide surface, a 532 nm diode-pumped solid-state laser and 640 nm diode laser (Oxxius, L6Cc) were directed to the surface with an incidence angle below the critical angle via a prism installed above the slide. Fluorescence signals of Cy3 and Cy5 dyes collected by an objective lens (Nikon, CFI Plan Apochromat VC 60X WI) placed below the quarts sample chamber were spectrally divided by a dichroic mirror (Chroma, T635lpxr) after removing scattered laser light by a laser blocking filter (Semrock, NF03-405/488/532/635E-25). The fluorescence signals were further cleared by bandpass filters (Chroma, ET585/65m for Cy3 and ET655LP for Cy5) and imaged on a sCMOS camera (Photometrics, PrimeBSI). The two lasers were operated with a trigger signal generated by the sCMOS camera for ALEX illumination scheme[43]. All the instruments were controlled by using commercial software (NIS elements, Nikon).

Single-molecule flow cell preparation and data acquisition

All single-molecule FRET experiments were performed at room temperature. The flow cells were prepared using our published protocol[19]. Briefly, quartz slides (G. Finkerbeiner Inc) were etched using acidic piranha and passivated with polyethylene glycol (PEG) to minimize any non-specific binding of molecules. mPEG-SVA and PEG-Biotin (Layson Bio) were used for the PEGylation. 50ul of 0.1mg/ml streptavidin (Thermofisher) was incubated into the flow channel for 5min. Excess was removed using 100 µL T50 (50mM Tris-HCl, pH 8.0, 50 mM NaCl). Next, 50 µL of 100pM biotinylated samples was introduced and incubated for 5min in the channel: linear DNA (Fig. 2), triangles (Fig. 3), or biotinylated Anti-His antibody (Extended Data Fig. 5c and d). Unbound molecules were washed away with 100 µL T50. 100 µL of 10 nM donor labeled imager strands and 100 nM of acceptor labeled imager strands against the sequences under investigation were injected in imaging buffer (50 mM TrisHCl, pH 8.0, 500 mM NaCl, PCD (Merck), PCA (Merck) and 1 mM 6-hydroxy-2,5,7,8-tetramethylchroman-2-carboxylic acid (Trolox) (Sigma). See Supplementary Table 1 for the full list of docking and imager strands.

Generally, for single-molecule studies, immobilization is carried out by biotin-streptavidin interactions[42]. However, it is highly difficult to precisely control the number of biotin molecules on the traditionally passivated surfaces (with Biotin-PEG). This raises the possibility of 2 or more binding pockets of streptavidin being occupied by biotins on the slide, leaving only one or two for actual fingerprinting. Thus, we modified the immobilization strategy for tetravalent and divalent streptavidin experiments (Fig. 4): Quartz slides were sonicated for >15min in Acetone, Methanol, and finally 1M KOH with washes with MilliQ in between. Next, the slides were flamed using a burner to remove organic residue if any, and immediately placed back in MilliQ. Finally, the slides were dried using a nitrogen blowgun and used for making the flow cell as explained above. The unused slides were stored at RT. 50ul of 1mg/ml of BSA-Azide (Click chemistry tools, 1535) was incubated with 15ul of 100uM (5') DBCO-DNA-Biotin (3') overnight in the dark at room temperature. 10nM of the resultant BSA-DNA-Biotin was added (50ul total volume) to the flow-cell and incubated for 10min. Excess BSA and free DNA were removed with 100ul T50. Next, 50ul of 1nM tetravalent or divalent Streptavidin was added to the channel and incubated for 5min. The excess was washed with 100ul of T50. Next, 100nM biotinylated docking strands were added to the flow cell and incubated for 30 min to ensure the labeling of all the streptavidin pockets. Unbound DNA was washed away with 100 µL T50. Following, 50 µL of 10 nM donor-labeled imager strands and 100 nM of acceptor-labeled imager strands prepared in the imaging buffer were injected into the flow cell.

Single-molecule fluorescence and FRET data analysis

The data collection and analysis were performed in multiple steps as reported previously[19]. A custom Python script was used to extract time traces of individual molecules from a sCMOS image collected at 0.1s exposure time per frame. Two-state K-means clustering algorithm were applied to the Cy3 and Cy5 fluorescence intensity traces to detect individual binding events of fluorescence imager strands. In order to ensure accurate results, binding events lasting for three or more consecutive frames were selected for further analysis. FRET efficiencies were calculated for each imager strand binding event and used to construct the FRET kymograph and histogram. From the events in which the acceptor probe dissociated or photobleached before the donor probe, we calculated the beta (leakage) and gamma correction factors for accurate FRET efficiency calculation following the method reported in a previous study [Biophysical Journal 99, 961–970]. Gaussian mixture modeling was applied to automatically classify populations in the FRET histogram. The Python-based automated analysis code can be freely accessed at the following link: https://github.com/kahutia/transient_FRET_analyzer2.

References

1. Dill, K.A. & MacCallum, J.L. The protein-folding problem, 50 years on. *Science* **338**, 1042-6 (2012).
2. Redler, R.L., Das, J., Diaz, J.R. & Dokholyan, N.V. Protein Destabilization as a Common Factor in Diverse Inherited Disorders. *J Mol Evol* **82**, 11-6 (2016).
3. Niroula, A. & Vihinen, M. Harmful somatic amino acid substitutions affect key pathways in cancers. *BMC Med Genomics* **8**, 53 (2015).

4. Teng, S., Srivastava, A.K., Schwartz, C.E., Alexov, E. & Wang, L. Structural assessment of the effects of amino acid substitutions on protein stability and protein protein interaction. *Int J Comput Biol Drug Des* **3**, 334-49 (2010).
5. Juritz, E. et al. On the effect of protein conformation diversity in discriminating among neutral and disease related single amino acid substitutions. *BMC Genomics* **13 Suppl 4**, S5 (2012).
6. Liu, J.J. et al. The structure-based cancer-related single amino acid variation prediction. *Sci Rep* **11**, 13599 (2021).
7. Shi, Y. A glimpse of structural biology through X-ray crystallography. *Cell* **159**, 995-1014 (2014).
8. Nogales, E. & Scheres, S.H. Cryo-EM: A Unique Tool for the Visualization of Macromolecular Complexity. *Mol Cell* **58**, 677-89 (2015).
9. Lerner, E. et al. Toward dynamic structural biology: Two decades of single-molecule Forster resonance energy transfer. *Science* **359**(2018).
10. Henzler-Wildman, K.A. et al. Intrinsic motions along an enzymatic reaction trajectory. *Nature* **450**, 838-44 (2007).
11. Sikic, K., Tomic, S. & Carugo, O. Systematic comparison of crystal and NMR protein structures deposited in the protein data bank. *Open Biochem J* **4**, 83-95 (2010).
12. Doerr, A. Single-particle cryo-electron microscopy. *Nat Methods* **13**, 23 (2016).
13. Nakane, T. et al. Single-particle cryo-EM at atomic resolution. *Nature* **587**, 152-156 (2020).
14. Lerner, E. et al. FRET-based dynamic structural biology: Challenges, perspectives and an appeal for open-science practices. *Elife* **10**(2021).
15. Yao, Y., Docter, M., van Ginkel, J., de Ridder, D. & Joo, C. Single-molecule protein sequencing through fingerprinting: computational assessment. *Phys Biol* **12**, 055003 (2015).
16. Clamme, J.P. & Deniz, A.A. Three-color single-molecule fluorescence resonance energy transfer. *Chemphyschem* **6**, 74-7 (2005).
17. Kummerlin, M., Mazumder, A. & Kapanidis, A.N. Bleaching-resistant, Near-continuous Single-molecule Fluorescence and FRET Based on Fluorogenic and Transient DNA Binding. *Chemphyschem* **24**, e202300175 (2023).
18. Vermeer, B. & Schmid, S. Can DyeCycling break the photobleaching limit in single-molecule FRET? *Nano Res* **15**, 9818-9830 (2022).
19. Filius, M., Kim, S.H., Severins, I. & Joo, C. High-Resolution Single-Molecule FRET via DNA eXchange (FRET X). *Nano Lett* **21**, 3295-3301 (2021).
20. Hohng, S., Joo, C. & Ha, T. Single-molecule three-color FRET. *Biophys J* **87**, 1328-37 (2004).
21. Lee, N.K. et al. Three-color alternating-laser excitation of single molecules: monitoring multiple interactions and distances. *Biophys J* **92**, 303-12 (2007).
22. Uphoff, S. et al. Monitoring multiple distances within a single molecule using switchable FRET. *Nat Methods* **7**, 831-6 (2010).
23. Kim, S.H., Kim, H., Jeong, H. & Yoon, T.Y. Encoding Multiple Virtual Signals in DNA Barcodes with Single-Molecule FRET. *Nano Lett* **21**, 1694-1701 (2021).
24. Durairaj, J., Akdel, M., de Ridder, D. & van Dijk, A.D.J. Geometricus represents protein structures as shape-mers derived from moment invariants. *Bioinformatics* **36**, i718-i725 (2020).
25. Sadler, E.E., Kapanidis, A.N. & Tucker, S.J. Solution-Based Single-Molecule FRET Studies of K(+) Channel Gating in a Lipid Bilayer. *Biophys J* **110**, 2663-2670 (2016).
26. Mendoza, V.L. & Vachet, R.W. Probing protein structure by amino acid-specific covalent labeling and mass spectrometry. *Mass Spectrom Rev* **28**, 785-815 (2009).

27. Kiselar, J.G. & Chance, M.R. Future directions of structural mass spectrometry using hydroxyl radical footprinting. *J Mass Spectrom* **45**, 1373-82 (2010).
28. Schneider, M., Belsom, A. & Rappsilber, J. Protein Tertiary Structure by Crosslinking/Mass Spectrometry. *Trends Biochem Sci* **43**, 157-169 (2018).
29. Yu, C. & Huang, L. Cross-Linking Mass Spectrometry: An Emerging Technology for Interactomics and Structural Biology. *Anal Chem* **90**, 144-165 (2018).
30. Fairhead, M., Krndija, D., Lowe, E.D. & Howarth, M. Plug-and-play pairing via defined divalent streptavidins. *J Mol Biol* **426**, 199-214 (2014).
31. Berntsson, R.P., Smits, S.H., Schmitt, L., Slotboom, D.J. & Poolman, B. A structural classification of substrate-binding proteins. *FEBS Lett* **584**, 2606-17 (2010).
32. Schuurman-Wolters, G.K. & Poolman, B. Substrate specificity and ionic regulation of GlnPQ from Lactococcus lactis. An ATP-binding cassette transporter with four extracytoplasmic substrate-binding domains. *J Biol Chem* **280**, 23785-90 (2005).
33. Fulyani, F. et al. Functional diversity of tandem substrate-binding domains in ABC transporters from pathogenic bacteria. *Structure* **21**, 1879-88 (2013).
34. de Boer, M. et al. Conformational and dynamic plasticity in substrate-binding proteins underlies selective transport in ABC importers. *Elife* **8**(2019).
35. Gouridis, G. et al. Conformational dynamics in substrate-binding domains influences transport in the ABC importer GlnPQ. *Nat Struct Mol Biol* **22**, 57-64 (2015).
36. Kummerlin, M., Mazumder, A. & Kapanidis, A.N. Bleaching-resistant, Near-continuous Single-molecule Fluorescence and FRET Based on Fluorogenic and Transient DNA Binding. *Chemphyschem*, e202300175 (2023).
37. MacDonald, J.I., Munch, H.K., Moore, T. & Francis, M.B. One-step site-specific modification of native proteins with 2-pyridinecarboxyaldehydes. *Nat Chem Biol* **11**, 326-31 (2015).
38. de Lannoy, C.V., Filius, M., van Wee, R., Joo, C. & de Ridder, D. Evaluation of FRET X for single-molecule protein fingerprinting. *iScience* **24**, 103239 (2021).
39. Krall, N., da Cruz, F.P., Boutureira, O. & Bernardes, G.J. Site-selective protein-modification chemistry for basic biology and drug development. *Nat Chem* **8**, 103-13 (2016).
40. Ruff, K.M. & Pappu, R.V. AlphaFold and Implications for Intrinsically Disordered Proteins. *J Mol Biol* **433**, 167208 (2021).
41. Kantner, T., Alkhawaja, B. & Watts, A.G. In Situ Quenching of Trialkylphosphine Reducing Agents Using Water-Soluble PEG-Azides Improves Maleimide Conjugation to Proteins. *ACS Omega* **2**, 5785-5791 (2017).
42. Roy, R., Hohng, S. & Ha, T. A practical guide to single-molecule FRET. *Nat Methods* **5**, 507-16 (2008).
43. Kapanidis, A.N. et al. Alternating-laser excitation of single molecules. *Acc Chem Res* **38**, 523-33 (2005).

Figures

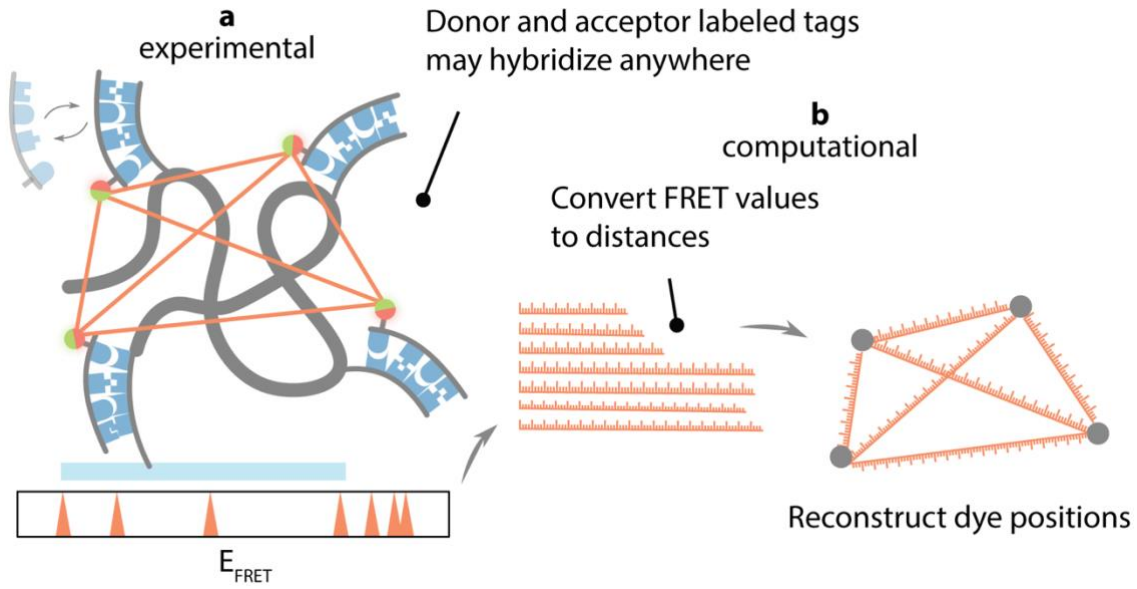

Fig. 1: The general concept of iMAX FRET.

a, Experimental module: A biomolecule consists of 2-4 coordinates carrying weak binder targets, here DNA docking strands to which cognate imagers can reversibly bind. The imagers are labeled with either donor or acceptor (green as donor and red as acceptor), and they both compete for the binding sites. Each successful FRET event has a particular FRET efficiency (E_{FRET}) between two coordinates and, over time, all possible FRET efficiencies accumulate to give rise to the FRET histogram.

b, Computational module - the apparent FRET efficiencies (E_{FRET}) for single molecules are converted into distances. They are run through geometrical reconstruction to predict the most optimal fit for the structure. This designates the predicted structure calculated based on the apparent FRET efficiencies.

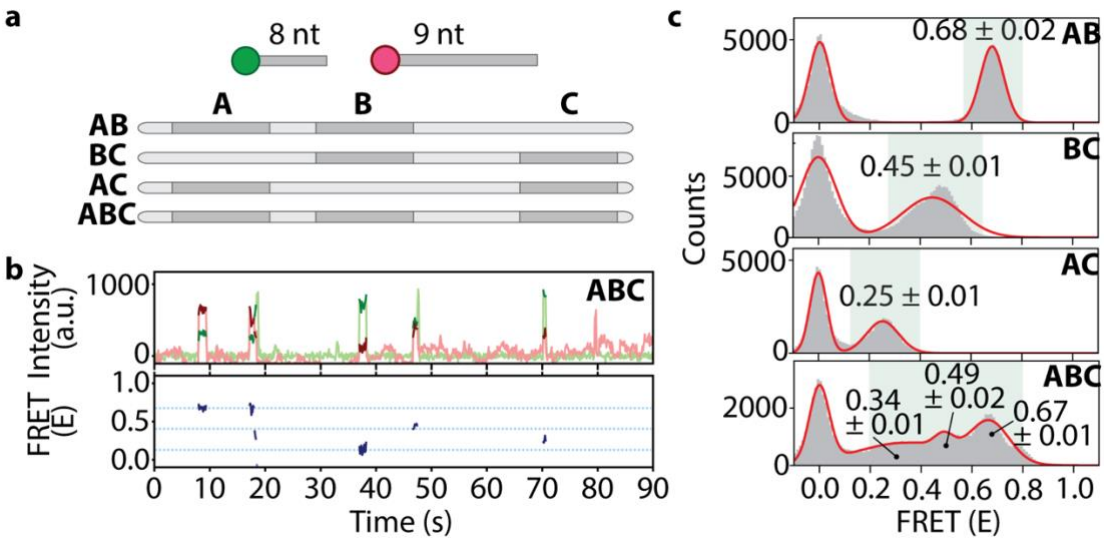

Fig. 2: Resolution of three targets in linear DNA using iMAX FRET.

a, Schematic representations of the linear DNA constructs. A, B, and C are the positions of identical docking sequences to which an 8nt donor- and a 9nt acceptor-labeled imager can bind. The molar ratio of the donor and acceptor strands were 1:10 (donor: acceptor). AB, BC, and AC are control constructs lacking either one of the three docking sequences, whereas ABC contains all three. The distances between A-B, B-C, and A-C are 12nt, 19nt, and 28nt, respectively.

b, Representative single-molecule intensity vs. time trace (top panel) for the ABC construct (green for donor and red for acceptor intensities). Note that there are three different intensity peaks for the red i.e. acceptor intensity showing FRET events corresponding to successful donor-acceptor imager pair binding to A-C, B-C, and A-C docking sequences. The bottom panel shows the marked FRET efficiencies in blue. The highest blue line corresponds to A-B FRET, the middle line to B-C FRET while the lowest designates the A-C FRET event.

c, Single-pair FRET event histograms from all molecules in a single field of view (grey bars). The mean FRET ± SEM is given for each peak in the histogram except the peak at 0.0 which corresponds to the donor-only binding events. Red solid lines are multi-Gaussian fit to the histograms. The FRET efficiency of each peak represents the distance between the designated docking sequences. Note the three peaks in the ABC construct corresponding to the three distances for A-C (0.34 ± 0.01), B-C (0.49 ± 0.01), and A-B (0.67 ± 0.01).

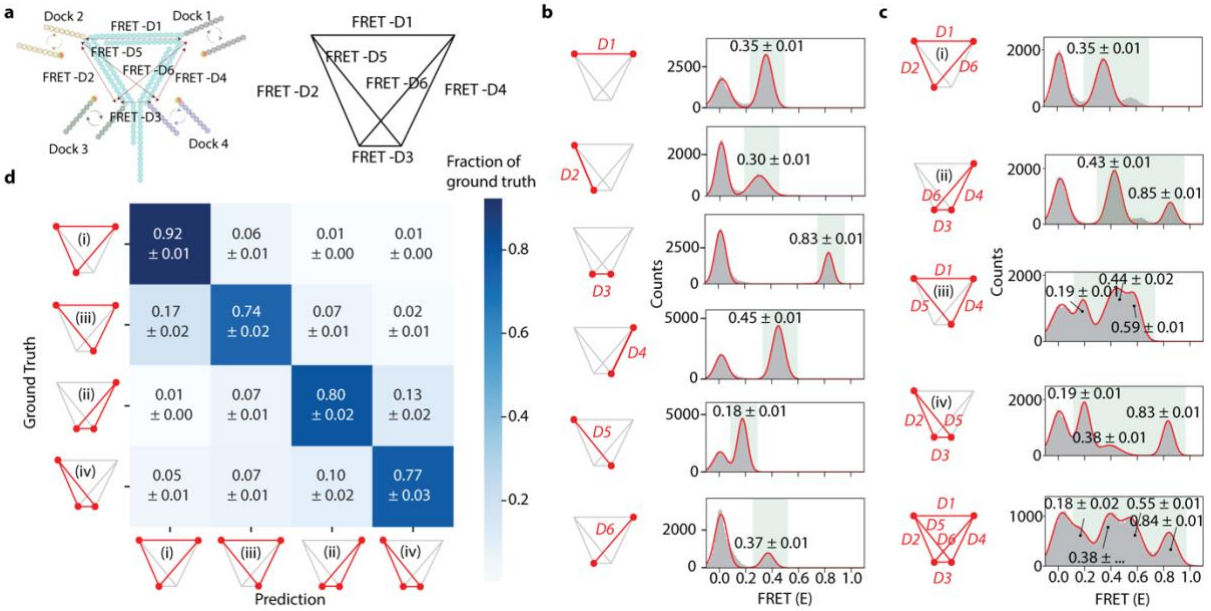

Fig. 3: iMAX FRET provides structural analysis of a complex DNA nanostructure.

a, Schematic representation of DNA nanostructure containing 4 overhangs of different DNA sequences which act as docking segments (Docks) for the imagers. As cognate imagers labeled with a donor or acceptor dye bind transiently to the Docks, FRET events occur in proportion to the distances between the Docks. 15 bp DNA length separates each pair of Docks 1-2 and 2-3, whereas the 13bp segment separates the Docks 1-4 giving rise to FRET distances of FRET-D1, D2, and D4, respectively. As a result, Docks 3 and 4 are situated very close to each other giving rise to FRET-D3. The Docks 2-4 and 1-3 also make a pair culminating in FRET-D5 and -D6, respectively. The right panel is the line representation of all the distances generated from the DNA nanostructure and will be used henceforth as a model figure.

b, iMAX FRET histograms of each FRET distance D1 to D6, separately. The red lines signify the FRET distance, red dots represent the Docks. Note that D1, D2, D4, and D6 are similar while FRET D2 and D3 mark the extremes in either direction. The shorter length of DNA (FRET D4, 13bp) is reflected in slightly higher FRET efficiency (0.45 ± 0.01) as opposed to 2bp longer FRET D1 and D2 (0.35±0.01 and 0.30±0.01), respectively. This hints at the distorted nanostructure due to differential side lengths.

c, iMAX FRET histograms for combinations of all 3 spatial points forming triangles (i-iv). The red lines signify the FRET distances, red dots represent the Docks. Note that triangle (i) has one mid-FRET degenerate peak due to the three overlapping distances of D1, D2, and D6. Triangle (iv) has one mid-FRET degenerate peak from D4 and D6, and a high-FRET peak arising from D3. The bottom structure contains four peaks with 2 degenerate peaks and 2 single peaks as a result of all the FRET distances D1-D6.

d, Confusion matrix showing classification accuracy and error modes of a tree-based machine learning classifier trained to identify the four triangles (i-iv) on a single molecule level and tested on held-out molecules. Each row denotes which fraction of total molecules for a given ground truth class are ascribed to which class, where the diagonal denotes correct classifications (i.e. the per-class accuracies).

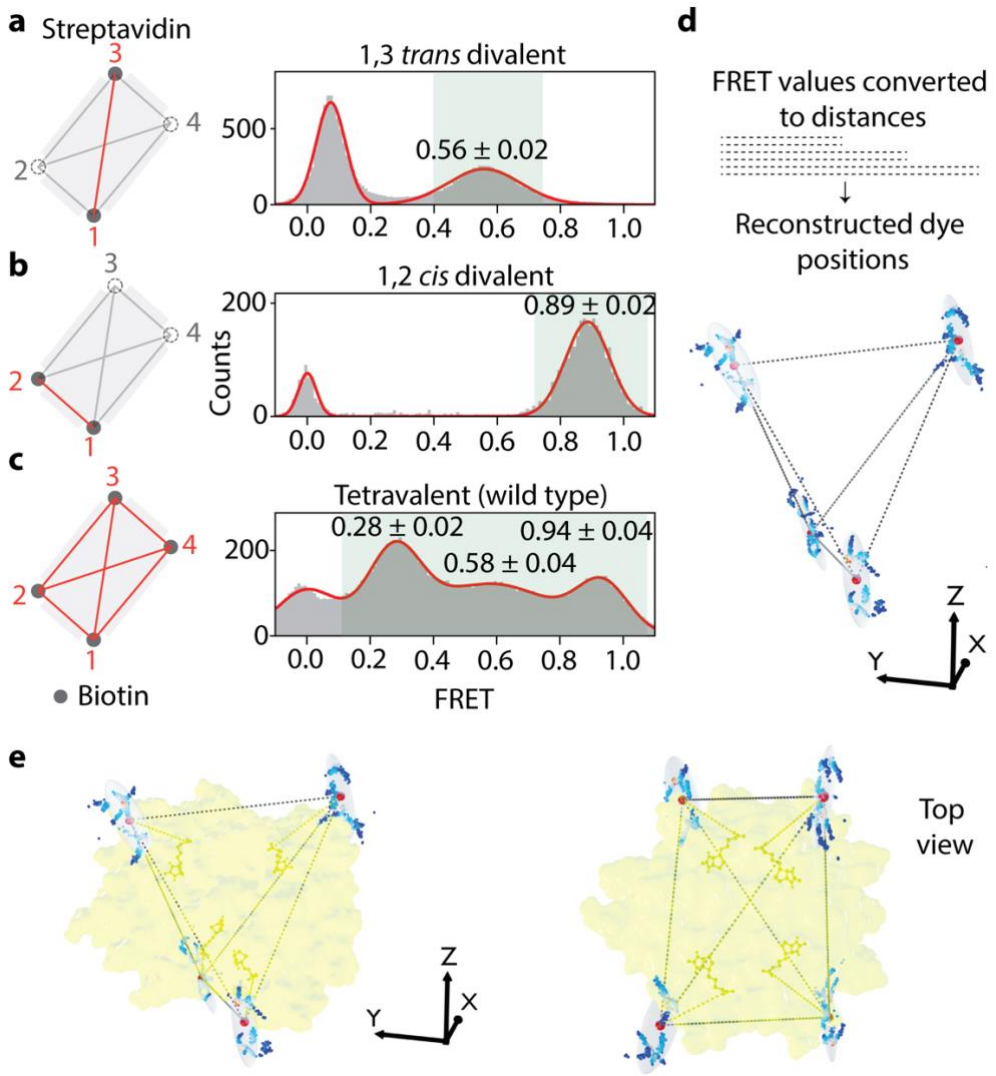

Fig. 4: **iMAX FRET-based structural analysis of streptavidin complexes.**
a, The mutant *1,3 trans* divalent streptavidin (PDB ID: 4BX6) that can bind biotin (grey dots) to only two binding pockets, whereas the other two are mutated to abrogate the biotin-binding (dashed circles). Upon binding of an imager, the dye is facing towards the binding pocket. The distance between the bound biotins (red line) shows the FRET efficiency of 0.56 ± 0.02 in the histogram.
b, The mutant *1,2 cis* divalent streptavidin (PDB ID: 4BX5) that can bind biotin as shown. The distance between the bound biotins (red line) shows a high FRET efficiency of 0.89 ± 0.02.
c, The wild-type tetravalent with four active biotin-binding pockets. Hence, it can give rise to six distance possibilities [n(n-1)/2]. However, streptavidin is a symmetrical molecule, hence shows three degenerate peaks, each peak corresponding to two overlapping peaks.
d, The FRET values are converted to six distances, and a structure is reconstructed for four biotin-binding pockets. Average positions for 1000 bootstrap iterations over all molecules are shown as dots (colored by density), the mean position is shown as a large red sphere and ovals report one standard error intervals (on average, 2.75Å).

e, The reconstructed structure is fitted into the reported (PDB ID: 2IZF) crystallographic streptavidin structure (yellow). Note that all four biotins can be fitted into the biotin-binding pockets with high accuracy.

Extended Information

iMAX FRET (**I**nformation **M**axi**m**ized FRET) for multipoint single-molecule structural analysis

Bhagyashree S. Joshi[a], Carlos de Lannoy[a], Mark Howarth[b,c], Sung Hyun Kim[a,d*], Chirlmin Joo[a,d*]

[a]Kavli Institute of Nanoscience, Department of Bionanoscience, Delft University of Technology, Delft, The Netherlands

[b]Department of Biochemistry, University of Oxford, South Parks Road, Oxford OX1 3QU, UK

[c]Current address: Department of Pharmacology, University of Cambridge, Tennis Court Road, Cambridge, CB2 1PD, UK

[d]Department of Physics, Ewha Womans University, Seoul 03760, Republic of Korea

* Corresponding authors:
Chirlmin Joo, c.joo@tudelft.nl;
Sung Hyun Kim, S.H.Kim@tudelft.nl

Supplementary Methods

Monte Carlo simulations

In iMAX FRET, which has multiple identical docking sites, the chance of having single-pair FRET events, i.e. simultaneous binding of one cy3- and one cy5 probes, largely depends on the probe binding kinetics. Experimentally, the binding frequency and binding dwell time of a probe can be controlled by the concentration and the length of the DNA probe, respectively. To find the optimal condition that maximizes the chance of having FRET events, we carried out series of Monte Carlo simulations at various kinetic rates. We defined a system with three docking sites each of which had three states of 1) probe unbound, 2) cy3 probe bound and 3) cy5 probe bound states. Given transition rates of the two probes, each docking site of the system was allowed to freely transit between states 1 and 2 or states 1 and 3, but not between 2 and 3. Each simulation ran for 1-million-time steps from which we typically observed >5000 transitions. We then selected events in which the system entered into the single-pair FRET emitting state, in which only one cy3 and cy5 probe were bound among the three docking sites. After removing events that lasted shorter than three consecutive time steps, the number of the selected single-pair FRET events and the total time spent of the system in them were studied to understand the effect of probe binding kinetics. The simulation code was written in Matlab and freely available upon request.

Structure prediction and classification

A computational pipeline for the reconstruction of 3D-shapes and shape classification was implemented in Python 3.9. Briefly, the number of dyes is determined from the number of FRET efficiency values, which are translated to distances. Distances are used to construct all distinct distance matrices (*D*) using pre-computed index matrices. Each distance matrix is then converted to a coordinate matrix as follows[1]. We construct the Gramm matrix (*M*),

$$M_{ij} = \frac{D_{1j}^2 + D_{i1}^2 - D_{ij}^2}{2}$$

where *i,j* are row and column index respectively. After eigenvalue decomposition,

$$M = USU^T$$

the coordinate matrix *X* can be calculated by sorting U and S by descending order of eigenvalue size, taking the first 3 columns of *U* (*U*[:, :3]) and first 3 eigen values (*S*[:3]) and calculating:

$$X = U[:, :3]\sqrt{S[:3]}$$

Poorly fitting distance matrices generate negative eigenvalues and are excluded. Finally, the remaining coordinate matrices are calculated back to distance matrices, and the coordinate matrix for which distances are closest to the original FRET efficiency-derived distances is returned. The algorithm was implemented in numpy (v1.21.5)[2] with distance matrix calculation as implemented in scipy (v1.8.0)[3].

Numerical embedding of 3D shapes for classification was done using the Geometricus package (v0.3.0)[4]. Embedded coordinates were concatenated to the FRET fingerprint, after which a boosted tree classifier implemented using the XGBoost package (v.1.6.1)[5] was trained and tested on the data using a 10-fold cross validation scheme. The analysis code is freely available at https://github.com/cvdelannoy/iMAX-FRET.

Preparation of the custom DNA nanostructure for Förster radius fitting and classifier applicability analysis

The position of docking site 2 was changed to three different locations (Extended Fig. 4a) using click chemistry. To achieve this, alkyne handles were introduced into the DNA backbone at three different locations one at a time in separate constructs. The docking strand for site 2 was designed to contain an azide handle at its one end. The alkyne and azide-containing DNAs were reacted using copper-click chemistry. The clicked DNA products (cyan box, Extended Fig. 4b) were gel purified and then the triangles were assembled to generate three structurally similar nanostructures (Extended Fig. 4a, bottom left). The positional changes between the (variable) docking site 2 and the fixed docking site 3 were reflected in the FRET values (Extended Fig. 4c and d), while it remained constant for all the triangles for the undeviating distance between docking sites three and four (Extended Fig. 4e). We could similarly recapitulate the change in FRET values in three coordinates i.e. docking sites two, three and four (Extended Fig. 4f).

Conversion of FRET efficiency into the distance R

The following sixth-power relation between *R* and *E* was used to calculate the distance based on the experimentally acquired FRET efficiency.

$$E = \frac{1}{1 + (R/R_0)^6}$$

The Förster radius (R_0), a parameter that combines the influence of dye and medium properties, and relative dye orientations, was fitted using the above custom DNA construct with dyes positioned at known locations along one DNA arm (Extended Fig 4g).

DNA structure modeling for Förster radius fitting

The Förster radius (R_0) denotes the dye distance at which the FRET efficiency is 0.5 and constitutes an essential parameter for the accurate calculation of distances from FRET efficiencies[6]. It factors in dye quantum yields and relative orientations, and the refractive index of the medium. In many applications, it suffices to approximate this value as a constant, however in structural biology, this may lead to unacceptable discrepancies with actual distances, as the effect of local environment and setup is ignored. Here we have used an elegant experiment to determine R_0, using our DNA nanostructure. Briefly, we measure FRET efficiencies for four triangles, created by click-chemistry (detailed in Extended Fig. 4).

To determine the Förster radius for our experiments, a single side of the DNA nanostructure was outfitted with clicked docking strands at positions 4, 7, and 15th base from a reference position. FRET efficiencies between clicked docking strands, the reference position, and a third position at one of the other angles of the nanostructure were then measured. We then used a parameter optimization approach with a tree-based Parzen estimator (TPE)

implemented in the hyperopt package (v.0.2.7)[7] to estimate the Förster radius. Briefly, this algorithm generates randomized proposals for all one or more variable parameters within given ranges and chooses the combination that minimizes the objective function. The TPE constrains the parameter space based on objective values of previous rounds so that the next guess is more likely to return a lower objective value. Using this approach, we simultaneously fitted Förster radius, linker length, and two DNA geometry parameters (twist and axial rise) after 100 iterations. Here, DNA geometry parameters were allowed to vary slightly to account for unnatural stresses in the nanostructure. As an objective function, the squared sum of the difference between the modeled dye position after triangle construction using given FRET efficiencies (see above) and the expected position given the DNA geometry was used. Supplementary Table 2 denotes ranges, step sizes, and fitted values for all parameters.

Extended Figures

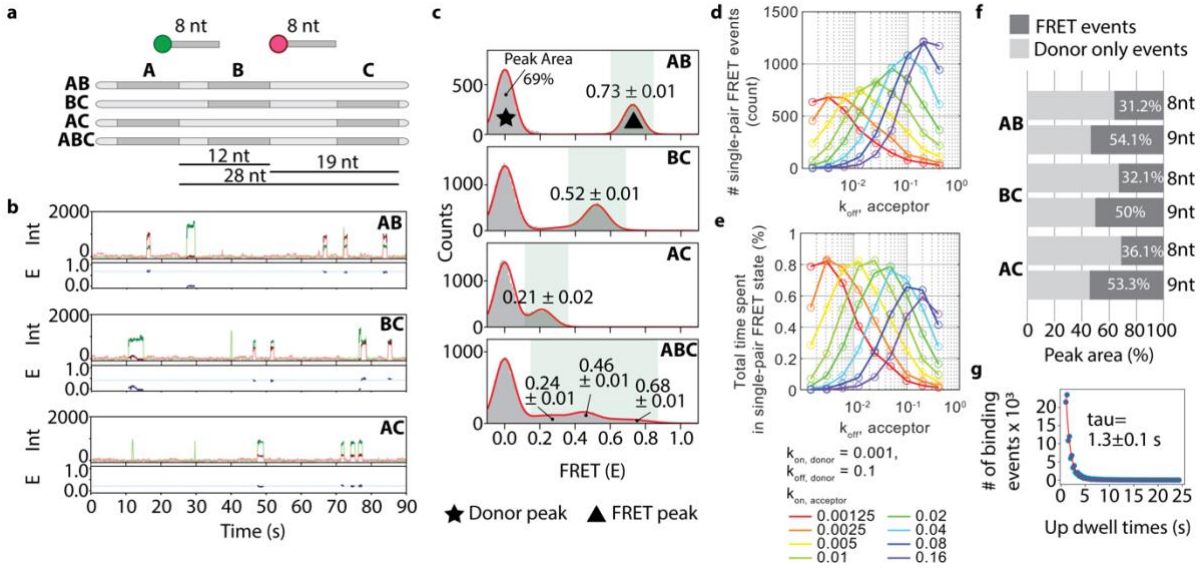

Extended Fig. 1: Rational design of the linear construct and imager characteristics for iMAX FRET.

a, Schematic representations of the linear DNA constructs. A, B, and C are the positions of identical docking sequences to which 8 nt donor- and acceptor-labeled imagers can bind. The donor to acceptor molar ratio was in a 1:10. The distances between the AB, BC, and AC segments are 12 nt, 19nt, and 28nt, respectively.

b, Single-molecule intensity time traces for donor (green), acceptor (red) and FRET (blue) for the linear constructs AB, BC, and AC.

c, Single-FRET event histograms from all molecules in a single field of view. Red solid lines are multi-Gaussian fit to the histograms. The three peaks in the ABC construct correspond to the three distances for A-C (0.24 ± 0.01), B-C (0.46 ± 0.01), and A-B (0.68 ± 0.01) (FRET ± SEM). Star designates the donor-only peak whereas the triangle reports the FRET evets peak.

d-e, The number of single-pair FRET events (d) and the total time spent (e) of a system with three docking strands, obtained from a series of Monte Carlo simulations with various probe binding kinetic rates. Given the donor binding ($k_{on,\ donor}$ = 0.001) and dissociation ($k_{off,\ donor}$ = 0.1) rates, the number of single-pair FRET events and total time spent within the state changed significantly with the acceptor binding ($k_{on,\ acceptor}$) and dissociation ($k_{off,\ acceptor}$) rates. While the maximum number of events were achieved with higher $k_{on,\ acceptor}$, the maximum time spent started decreasing when $k_{on,\ acceptor}$ was more than 10 times higher than that of the donor. At the optimal 10-times higher $k_{on,\ acceptor}$, $K_{off,\ acceptor}$ should be ~5-10 times lower than that of the donor to maximize the chance of observing single-pair FRET.

f, Peak areas for donor only- and single-FRET events for each linear construct are plotted as percentages. Note the increase of 1.5-fold in the FRET events peak area when a longer acceptor imager (9nt) is used instead of an 8nt imager.

g, Dwell time histogram of the 9nt acceptor imager binding events (Blue circles). The dwell time determined from single-exponential fit (red line) was 1.3±0.1 s under our experimental conditions (time ± SEM s)

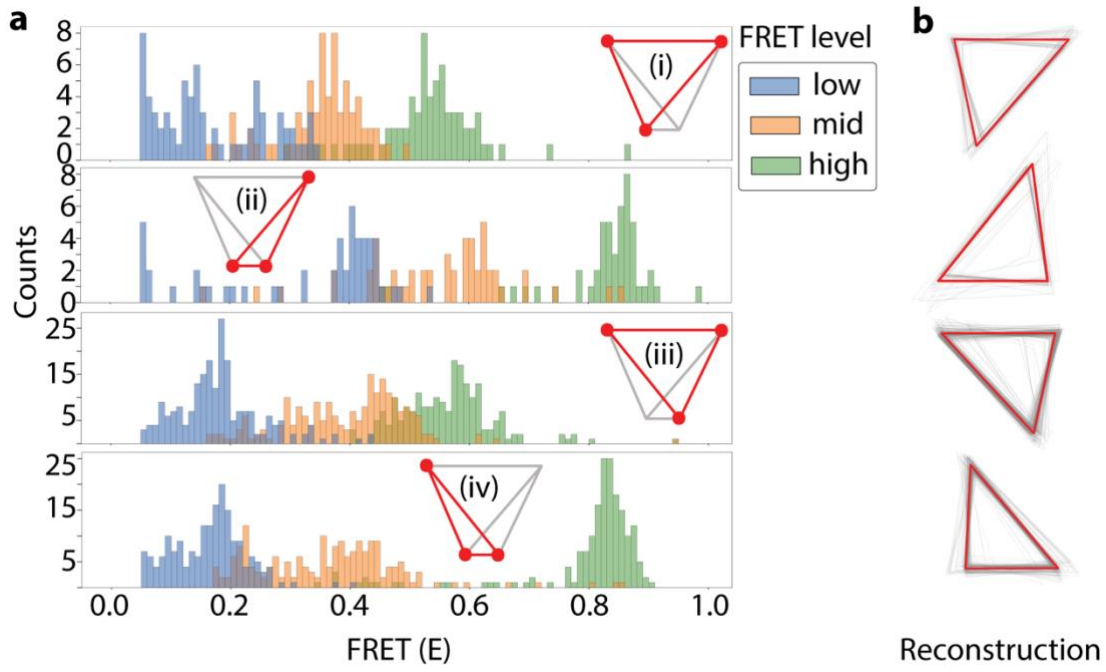

Extended Fig. 2: Reconstruction of triangles for single-molecule FRET histograms
a. Histograms displaying per-molecule FRET efficiencies separately for each of the three levels (low, mid, and high) per triangle type in the quadrangular DNA nanostructure (i to iv). Only molecules featuring all three values are shown.
b. Aligned reconstructed triangles for all single molecules (grey) and the average triangle (red) per triangle type.

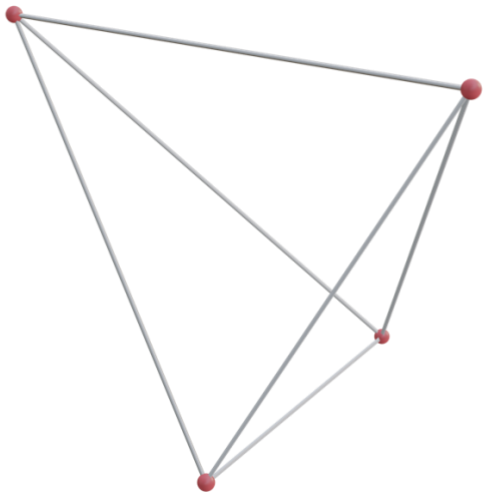

Extended Fig. 3: 3D reconstruction of the quadrangular DNA nanostructure
3D reconstruction of the relative dye positions in the nanostructure based on FRET values, revealing its assymetric and staggered nature.

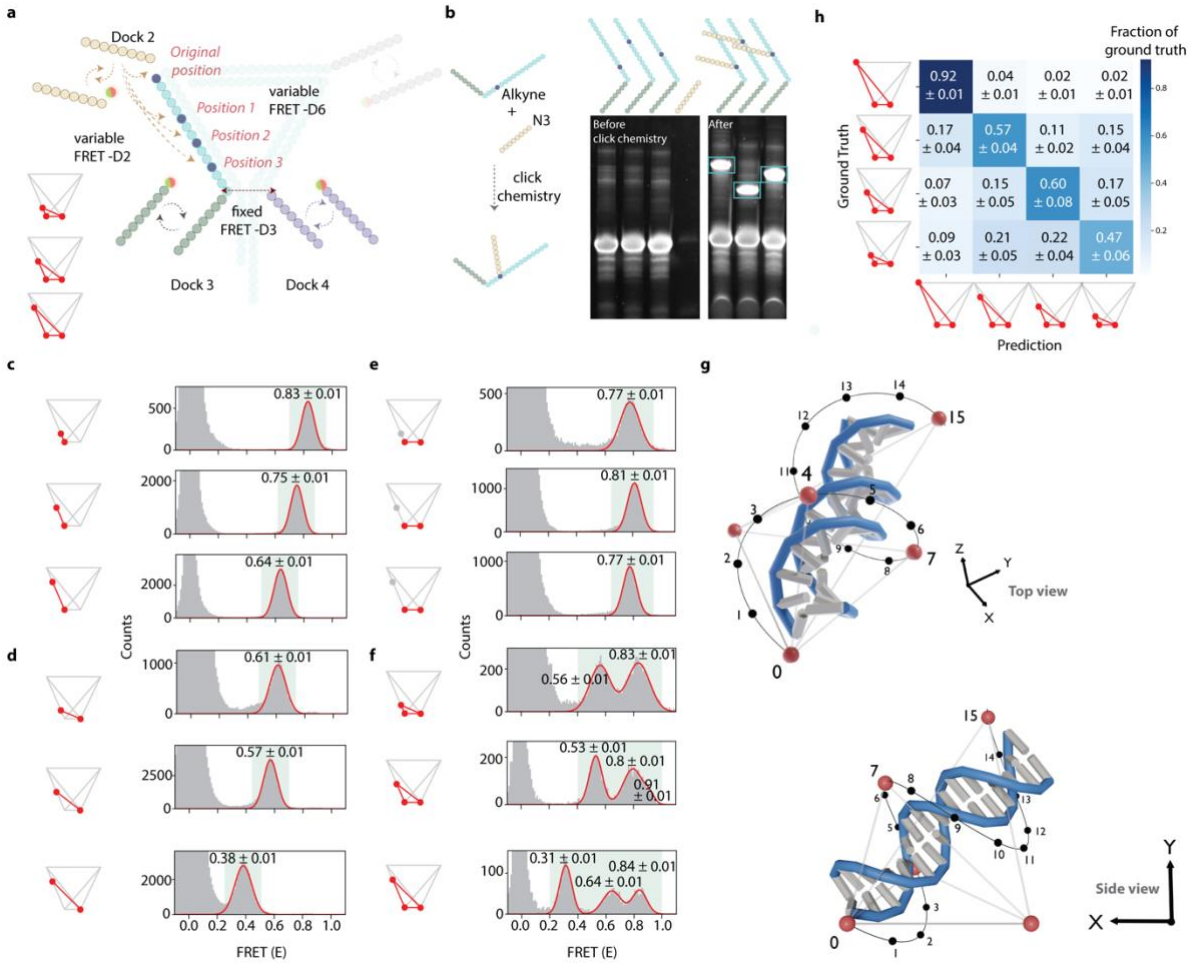

Extended Fig. 4: iMAX FRET-based analysis of closely related DNA nanostructures

a, In the complex DNA nanostructure, the position of Dock 2 is changed to three different positions giving rise to three FRET-D2 variations.

b, Click-chemistry is used to attach an azide-linked Dock 3 to the backbone DNA with an alkyne handle. The clicked DNA products (cyan box) were gel extracted and then the nanostructures were reconstituted by hybridization.

c, The FRET changes between the (variable) Dock 2 and fixed Dock 3 are reflected in the change in the differential position change of Dock 2.

d, The changes in Dock 2 also changed the distance between sites 2 and 4, as confirmed by the changing FRET values.

e, FRET values for the distances, between sites 3 and 4, as expected, remained majorly unaffected.

f, The change in FRET values in three points can be similarly recapitulated, for the triangles with imagers and Docks 2,3, and 4. Overall FRET values also shifted for triangles as well for all positions with respect to the original triangle (iv).

g, 3D reconstruction of dsDNA strand (blue/white) with dye positions (red spheres) of three triangles with the same base reconstructed from FRET efficiencies. Triangles differed in the position of their third dye, which was located at nucleotides with indices 4, 7, or 15, counted from the base. Förster radius, DNA twist, DNA axial rise, and dye-DNA linker length were optimized using a tree-based Parzen estimator-based approach. Black numbers and dots denote expected dye positions and indices for linkers attached to different nucleotides, based

on DNA geometry and linker length. Images rendered at two different view angles were generated in Blender (v3.6).

h, our integrated computational approach can differentiate the 3D structures from each other on a single molecule level with up to 60% accuracy.

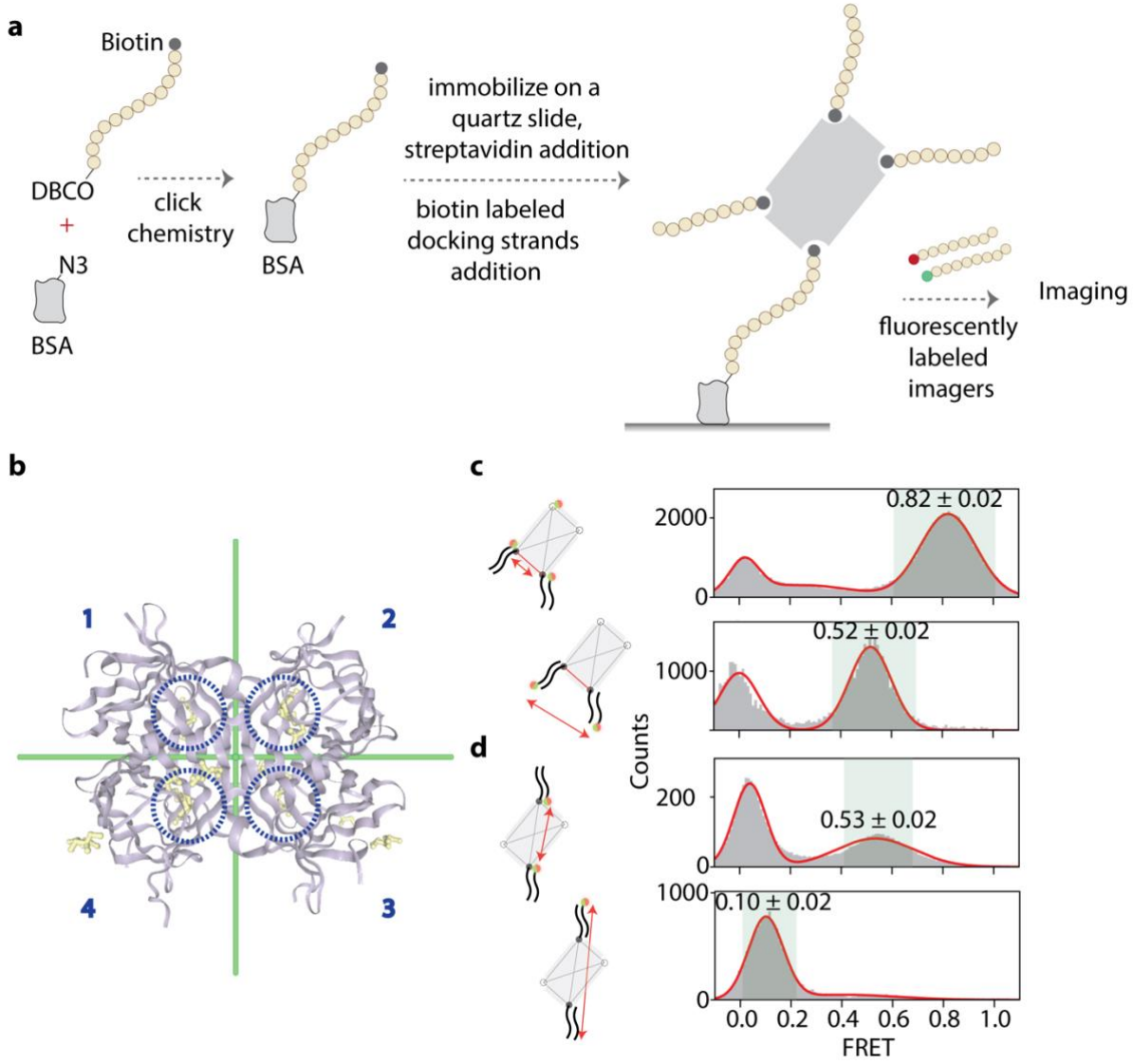

Extended Fig. 5: Immobilization Scheme of streptavidins and their structural analysis

a, BSA-Azide was immobilized on a quartz slide, conjugated with DNA with a DBCO handle at one end and biotin at the other. The presence of only one Azide per BSA molecule allowed the attachment of one biotin, and thus one streptavidin molecule per BSA molecule. Using this newly developed immobilization scheme, we could ensure that only one pocket is filled with biotin for immobilization and that the remaining 3 pockets are available for binding biotinylated docking sequences for fingerprinting.

b, D2 symmetry of the wild-type streptavidin tetramer (from PDB ID: 3RY2). 1,2,3 and 4 designate the numbering of subunits in the tetramer. Biotins (yellow space fills) are highlighted with dashed blue circles.

c and d, With the use of imagers for probing as opposed to covalently conjugated dyes generally used in FRET assays, we could modify the location of dye to artificially change the distance between the 2 points. When 3' instead of 5' dye-labeled imagers were applied, we could see the relative FRET shift to lower efficiencies corresponding to the new distance, on the divalent structures. 1,2 cis divalent streptavidin shows a change of 0.30 FRET value, while it is 0.43 for the 1,3 trans divalent streptavidin mutants.

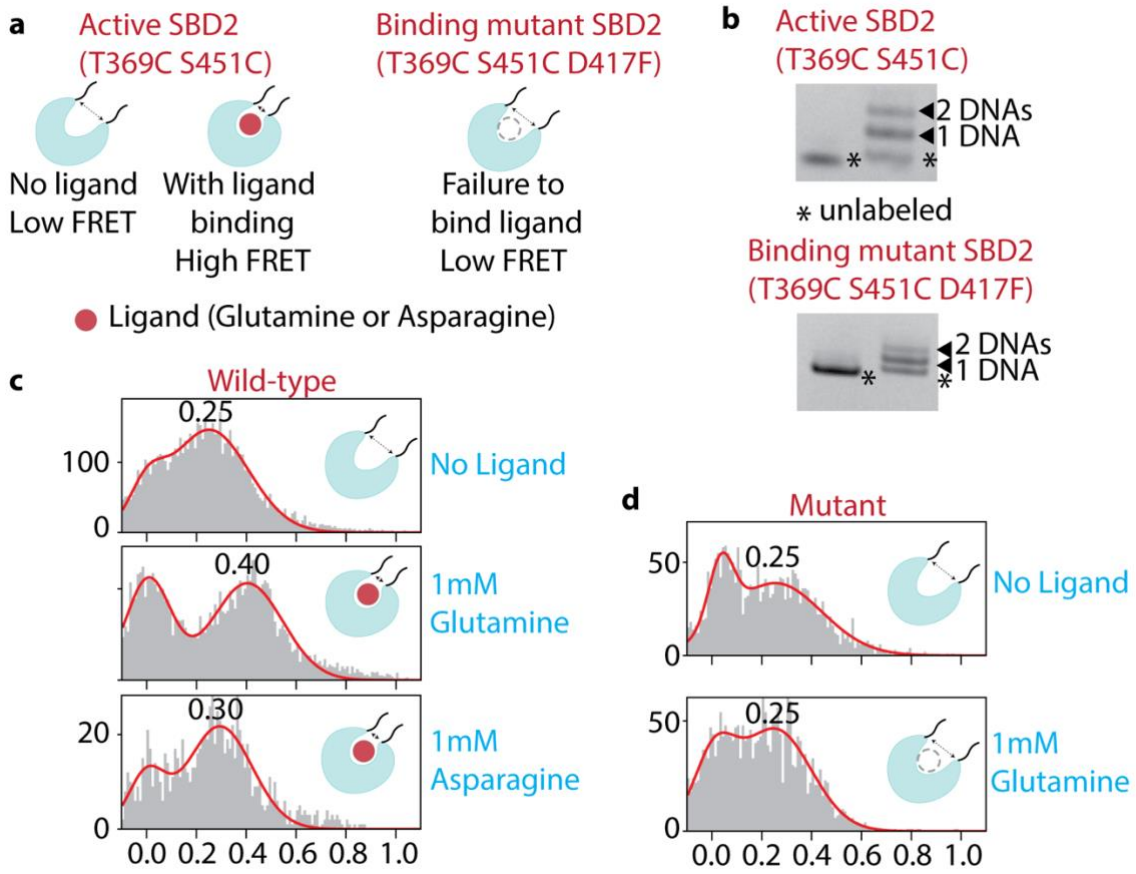

Extended Fig. 6: Structural analysis of conformational changes in SBD2-ligand complexes
a, 2 mutant SBD2 proteins – active (T369C S451C) and null (T369C S451C D417F). The cysteines are strategically added for DNA labeling. When a cognate ligand is bound, the conformation change results in higher FRET. Whereas, the null mutant retains the low-FRET value due to a lack of ligand binding.
b, The SBD2 proteins are labeled with DNA using click chemistry. The ladder pattern suggests the weight shift due to the addition of one or both DNAs attached to the protein.
c, The SBD2 protein changes its 0.25 FRET value (no ligand) to 0.40 upon its preferred glutamine ligand binding. When Asparagine is added, it stabilizes at 0.30 FRET.
d, The mutant SBD2, due to the inability of ligand binding remains at 0.25 FRET after the application of glutamine.

Supplementary Tables

Supplemetary Table 1: DNA constructs

Corresponding Fig.	Description	Sequence (5'-3')	Modification	Supplier
Fig. 2	Linear construct with POI-A and B docking sequences	ttttttttttttttttttttATACAT CTAtttATACATCTA	5' Biotin	Ella Biotech (GmbH)
Fig. 2	Linear construct with POI-B and C docking sequences	tttttATACATCTAttttttttA TACATCTAttttttttttt	5' Biotin	Ella Biotech (GmbH)
Fig. 2	Linear construct with POI-A and C docking sequences	tttttATACATCTAttttttttt ttttttttATACATCTA	5' Biotin	Ella Biotech (GmbH)
Fig. 2	Linear construct with POI-A, B and C docking sequences	tttttATACATCTAttttttttA TACATCTAtttATACATCT A	5' Biotin	Ella Biotech (GmbH)
Fig. 2	Donor imager strand	AGATGTAT	3' Cy3	Ella Biotech (GmbH)
Fig. 2	Acceptor imager strand	AGATGTAT	3' Cy5	Ella Biotech (GmbH)
Fig. 2	Longer acceptor imager strand	TAGATGTAT	3' Cy5	Ella Biotech (GmbH)
Fig. 3	DNA Nanostructure left arm + Dock 1	AGAGG AGGAT TTCGG TACAC CCGAC AG	-	Ella Biotech (GmbH)
Fig. 3	DNA Nanostructure backbone + Dock 2	ATTCA TTCTC ATCCT CTGTC GGGTG TACCG TAAGG TGAAT AGTGA CTTTA TACAT CTA	-	Ella Biotech (GmbH)
Fig. 3	DNA Nanostructure biotin strand	CTGAT TGTTA TCGAG GATGA GAATG AATTT TTTTT TTTTT TTT	Biotin – 3'end labeled	Ella Biotech (GmbH)
Fig. 3	DNA Nanostructure right arm + Dock 4	TCTTC ATTAC TTTTC GATAA CAATC AGGTC ACTAT TCACC TTA	-	Ella Biotech (GmbH)
Fig. 3	DNA Nanostructure Left arm + Dock 2 and Dock 3	AGAGG AGGAT TTCGG TACAC CCGAC AGTTT TCAAT GTA	-	Ella Biotech (GmbH)
Fig. 3	DNA Nanostructure donor imager strand Dock 1	AGATGTAT	3' Cy3	Ella Biotech (GmbH)

Fig. 3	DNA Nanostructure acceptor imager strand Dock 1	TAGATGTAT	3’ Cy5	Ella Biotech (GmbH)
Fig. 3	DNA Nanostructure donor imager strand Dock 2	TCCTCCT	5’ Cy3	Ella Biotech (GmbH)
Fig. 3	DNA Nanostructure acceptor imager strand Dock 2	TCCTCCTC	5’ Cy5	Ella Biotech (GmbH)
Fig. 3	DNA Nanostructure donor imager strand Dock 3	TACATTGA	3’ Cy3	Ella Biotech (GmbH)
Fig. 3	DNA Nanostructure donor imager strand Dock 3	TACATTGAA	3’ Cy5	Ella Biotech (GmbH)
Fig. 3	DNA Nanostructure donor imager strand Dock 4	AGTAATGA	5’ Cy3	Ella Biotech (GmbH)
Fig. 3	DNA Nanostructure acceptor imager strand Dock 4	AGTAATGAAG	5’ Cy5	Ella Biotech (GmbH)
Extended Data Fig. 3	Clickable DNA Nanostructure Left arm + Dock 2 Position 4	CGGTACACCCGA7AGTTTTCAATGTA	7= C8-Alkyne-dC	Biomers.net (GmbH)
Extended Data Fig. 3	Clickable DNA Nanostructure Left arm + Dock 2 Position 2	CGGTA7ACCCGACAGTTTTCAATGTA	7= C8-Alkyne-dC	Biomers.net (GmbH)
Extended Data Fig. 3	Clickable DNA Nanostructure Left arm + Dock 2 Position 3	CGGTACACC7GACAGTTTTCAATGTA	7= C8-Alkyne-dC	Biomers.net (GmbH)
Extended Data Fig. 3	Clickable Dock 2	AGAGGAGGATTT	5’ Azide-pro	Biomers.net (GmbH)
Fig. 4	Docking strand for streptavidin WT and mutants	ATACATCTA	3’ Biotin	Ella Biotech (GmbH)
Fig. 4	Immobilization strand for streptavidin WT and mutants	AAAAGAAAAGAAATACATCTAT	5’ DBCO, 3’ Biotin	Ella Biotech (GmbH)
Extended Data Fig. 4	Docking strand for proteins – SBD2 WT and mutants	TATACATCTAT	5’ Azide-pro	Ella Biotech (GmbH)

Supplementary Table 2: **Förster radius fitting parameters**
Ranges, step sizes, and fitted values for all parameters fitted by the tree-based Parzen estimator optimization algorithm. Here, the structure diameter spans the DNA strand diameter and two times the linker length.

	Min	Max	Step size	Fitted value
Förster radius (Å)	50	60	0.1	53.8
DNA twist (°/bp)	32	40	1	39
Axial rise (Å/bp)	2.3	5.0	0.1	4.1
Structure diameter (Å)	25	70	0.5	38

References

1. Crippen, G.M., Havel, T. F., . Stable calculation of coordinates from distance information. *Acta Crystallographica Section A* **2**, 282-284 (1978).
2. Harris, C.R. et al. Array programming with NumPy. *Nature* **585**, 357-362 (2020).
3. Virtanen, P. et al. SciPy 1.0: fundamental algorithms for scientific computing in Python. *Nat Methods* **17**, 261-272 (2020).
4. Durairaj, J., Akdel, M., de Ridder, D. & van Dijk, A.D.J. Geometricus represents protein structures as shape-mers derived from moment invariants. *Bioinformatics* **36**, i718-i725 (2020).
5. Guestrin, T.C.a.C. XGBoost: A Scalable Tree Boosting System. *arXiv* (2016).
6. Hohlbein, J., Craggs, T.D. & Cordes, T. Alternating-laser excitation: single-molecule FRET and beyond. *Chem Soc Rev* **43**, 1156-71 (2014).
7. Bergstra, J., Yamins, D. & Cox, D. Making a Science of Model Search: Hyperparameter Optimization in Hundreds of Dimensions for Vision Architectures. in *Proceedings of the 30th International Conference on Machine Learning* Vol. 28 (eds Sanjoy, D. & David, M.) 115--123 (PMLR, Proceedings of Machine Learning Research, 2013).